Research Square

Preprints are preliminary reports that have not undergone peer review.
They should not be considered conclusive, used to inform clinical practice,
or referenced by the media as validated information.

Dbd Plasma Characterization for O_2 Production via Co_2/co Dissociation in Palm Oil Biomass Emission

Rahmad Oktafiansyah

rahmad.oktafiansyah@ulm.ac.id

Lambung Mangkurat University

Gusti Atika Urfa

Lambung Mangkurat University

Andi Tessiwoja Tenri Ola

Lambung Mangkurat University

Suryajaya Suryajaya

Lambung Mangkurat University

Muhammad Aghil Surya Syahputra

Lambung Mangkurat University

Muhammad Fadhil Syahputra

Lambung Mangkurat University

Muhammad Afief Balya

Lambung Mangkurat University

Research Article

Keywords: Plasma, Combustion, Oil palm

Posted Date: May 26th, 2026

DOI: https://doi.org/10.21203/rs.3.rs-9342983/v1

License: This work is licensed under a Creative Commons Attribution 4.0 International License.
Read Full License

Additional Declarations: No competing interests reported.

Version of Record: A version of this preprint was published at Water, Air, & Soil Pollution on August 19th, 2026. See the published version at https://doi.org/10.1007/s11270-026-09845-y.

Abstract

Combustion of oil palm empty fruit bunch biomass produced carbon dioxide and carbon monoxide emissions that were hard to clean-up using ordinary gas-cleaning methods. This study assessed the efficacy of a dielectric barrier discharge non-thermal plasma system to dissociate the gases from actual biomass-derived exhaust. The system consists of a gas-conditioning chamber, a plasma reactor, and an isolated measurement chamber for real-time monitoring. The applied voltage was varied from 19–23 V to examine the effect of discharge behavior on gas conversion. The results showed that operation with 21 V results the highest carbon dioxide dissociation and oxygen formation through efficient electron-impact processes in a diffuse discharge regime. At higher voltages, filamentary behavior made the system less efficient. The study demonstrated the potential of dielectric barrier discharge plasma for biomass emission treatment.

1. Introduction

The palm oil processing industry is one of the biggest sources of greenhouse gas emissions in Indonesia. This is mostly because it burns biomass waste like empty fruit bunches (EFB) (Hong 2023; Nabila et al. 2023). When EFB burns, the fuel gas that comes from it usually has a lot of CO_2 and CO, as well as water vapor, hydrocarbons, volatile organic compounds (VOCs), and particulate matter. The complex makeup of these emissions makes them worst for the environment and makes traditional gas-cleaning technologies ineffective (Dolah et al. 2021; Majesty et al. 2024; Sato et al. 2025). As country work harder to cut down on carbon emissions grow, it is becoming increasingly necessary to find effective, energy-efficient, and flexible ways to cut down on CO_2 and CO emissions from burning palm oil biomass (Al-Muraisy et al. 2025a).

When used in real industrial exhaust streams, conventional CO_2 management technologies, like chemical absorption, high-temperature catalysis, and solid sorbents, demonstrate significant limitations (Chai et al. 2022; Zentou et al. 2025). Amine-based absorbents need to be warmed up again and are sensitive to water and other impurities. Catalytic routes, on the other hand, need to stay at high temperatures and often stop working when tar and other particles are present. Because of these limits, it is hard to use regular systems in palm oil mills, where the gas composition, temperature, and humidity change a lot while they are running (Bui et al. 2018; Ren et al. 2025; X. Wang and Song 2020a).

Dielectric Barrier Discharge (DBD) and other non-thermal plasma technologies are great options for directly activating CO_2 and CO at low temperatures (Chang et al. 2022; Chen et al. 2025; Golubev et al. 2025). DBD plasmas yield very energetic electrons that can cause vibrational excitation, electronic excitation, and dissociative electron-impact reactions without raising the temperature of the bulk gas too much. These traits let plasma systems work well in conditions that are close to normal, which makes them great for treating industrial exhaust on site (Michielsen et al. 2017; Mukhtar et al. 2024).

Earlier research on DBD-based CO_2 conversion, mainly utilizing high-purity CO_2 or simplified gas mixtures, has yielded quantifiable dissociation yields, pinpointed essential electron-driven pathways, and

showcased improvements via plasma-catalytic and dielectric-packing arrangements (Lindon and Scime 2014; Michielsen et al. 2017; Ponduri et al. 2016a). However, the efficacy of DBD plasma in the context of actual biomass-derived fuel gas is still not fully comprehended. High humidity causes more radical chemistry, mostly by making OH and H; VOCs and tar vapors can start secondary oxidation reactions; and particulate deposition can change how evenly the discharge happens. These factors together change the reduced electric field (E/N), the distribution of electron energy, and the discharge mode, which in turn affects plasma reactivity. Consequently, the behavior of CO_2/CO dissociation in industrial exhaust cannot be directly extrapolated from laboratory studies utilizing controlled gas mixtures (A. Bogaerts et al. 2017; Korzec et al. 2025; Snoeckx and Bogaerts 2017; W. Wang et al. 2018).

This study utilized a DBD-based plasma system directly on EFB combustion exhaust under regulated low-pressure conditions. The system combines an emission-sampling chamber with a plasma treatment unit that lets you analyze gases in real time while the plasma is running. The study systematically varies the applied voltage to examine the transition between diffuse and filamentary discharge modes and assesses their impact on CO_2/CO conversion, O_2 generation, and competing radical-driven oxidation pathways. The research clarify plasma–flue-gas interactions under industry-relevant conditions, make standard for basis for enhancing plasma-based emission treatment in palm oil processing facilities.

2. Materials and Methods

The experimental system comprised of two integrated subsystems designated for the treatment and characterization of emission originating from biomass. The initial subsystem was a gas-conditioning chamber that gathered the combustion exhaust from an oil palm empty-fruit-bunch (EFB) burner and regulated the flow under controlled low-pressure conditions (Moliner et al. 2022). This chamber served to homogenize the gas mixture and ensure consistent setting of CO_2-, CO-, and VOC-rich biomass emissions to the plasma region (Al-Muraisy et al. 2025b; Purawiardi et al. 2025).

The second subsystem was a non-thermal dielectric barrier discharge (DBD) plasma unit that worked at atmospheric pressure and had an input voltage that could be changed. This module was developed to initiate electron-driven reactions capable of activating and dissociating CO_2 and CO without significant bulk heating (Lindon and Scime 2014; Ponduri et al. 2016a). Applied voltage was varied in the range of 19 to23 V to examine how it affected the behavior of the discharge and the transformation of the gas-phase.

An in-situ gas analysis module was positioned downstream of the DBD plasma zone and connected through a dedicated gas-transfer line to an isolated measurement chamber. This configuration ensured that the O_2, CO_2, and CO sensors were not exposed directly to the discharge region, thereby preventing electromagnetic interference, thermal perturbation, and premature sensor degradation (Annemie Bogaerts et al. 2018; Golubev et al. 2025; Kafi et al. 2023; X. Wang and Song 2020b). As a substitute, the plasma-treated exhaust was sent to the measuring chamber, where the gas composition was measured over time at different plasma input voltages. By separating the plasma reactor from the sensing

chamber, the system made it possible to accurately monitor the change of temporal concentration while keeping a controlled and stable detection environment (Jamaludin et al. 2024). This design also allowed real-time correlation between plasma operating parameters and the evolution of chemical species without revealing the proprietary internal integration architecture of the sensing system.

3. Results and Discussion

In this study, a DBD-based plasma system was directly utilized to EFB combustion exhaust under controlled low-pressure conditions. The system combines an emission-sampling chamber with a plasma treatment unit that allows designed to enable real-time gas analysis during plasma operation. By systematically varying the applied voltage, the study investigates the transition between diffuse and filamentary discharge modes and evaluates their influence on CO_2/CO conversion, O_2 formation, and competing radical-driven oxidation pathways (Mei et al. n.d.; Oktafiansyah et al. 2022; Soldatov et al. 2021). The work provides new insights into plasma-flue gas interactions under industrially relevant conditions, offering a foundation for optimizing plasma-based emission treatment in palm oil processing facilities.

The oxygen concentration profile shown in Fig. 1 exhibits a clear increase in O_2 formation up to approximately 21–22 V, after which the concentration gradually declines as the applied voltage continues to rise. A notable feature appears at the initial segment of the x-axis, where the O_2 concentration rises immediately after plasma ignition. This rapid onset indicates that the DBD plasma promptly initiates oxygen-producing reactions, in contrast to the untreated flue gas, where molecular oxygen does not emerge within the same short residence time. The instantaneous rise is attributed to non-equilibrium, electron-driven processes capable of generating atomic oxygen radicals on microsecond timescales processes that are not achievable under purely thermal or conventional gas-phase conditions typical of biomass combustion emissions (Elaissi and Alsaif 2023; Shaban et al. 2024).

Between 19 and 21 V, the discharge operates predominantly in a diffuse microdischarge regime. In this regime, the electric field is relatively uniform, resulting in spatially distributed microdischarges characterized by moderate electron temperatures and controlled electron energy distributions. The electron energy distribution function (EEDF) at these voltages favors vibrational excitation and dissociation of CO_2 rather than excessive ionization. As a consequence, electron-impact reactions efficiently generate O□ and O(¹D) radicals through CO_2 fragmentation (Alliati et al. n.d.-a; Ponduri et al. 2016b). These species act as the principal precursors for subsequent O_2 formation. Although O(¹D) is highly reactive, it rapidly relaxes to the ground-state O□ radical, which can recombine to form molecular oxygen, producing O_2 at rates consistent with the increasing trend observed in the low-to-mid voltage region. While reverse reactions involving CO and O□ still occur, they do not yet dominate the chemistry, allowing net O_2 production to continue rising. Under these diffuse-regime conditions, electron-impact dissociation of CO_2 remains the primary pathway for atomic oxygen generation in both ground and excited states, facilitating the observed enhancement in O_2 concentration, such as the following reaction (Aerts et al. 2015a; Alliati et al. n.d.-b; Hayakawa et al. 2023a):

$CO_2 + e^- \rightarrow CO + O(^3P)$ (1)

$CO_2 + e^- \rightarrow CO + O(^1D)$ (2)

$CO + O(^3P) \rightarrow CO_2$ (3)

$O(^3P) + O(^3P) + M \rightarrow \mathbf{O_2} + M$ (4)

As the voltage increases beyond 21–22 V, the discharge gradually transitions from the diffuse regime into a partially filamentary regime. Filament formation introduces narrow plasma channels with significantly higher local electron density and strong transient electric fields. This shift alters the EEDF by increasing the proportion of high-energy electrons and promoting localized heating. While these conditions can theoretically enhance CO_2 dissociation, they also accelerate competing reactions that rapidly consume atomic oxygen (Ozkan et al. 2016; Ray and Subrahmanyam 2016; Urfa et al. n.d.). In the context of palm-biomass flue gas, where substantial water vapor and volatile organics are present, $O(^3P)$ radicals are readily depleted through reactions with H_2O and VOC fragments. The intensified formation of $OH(^2\Pi)$ and oxidized organic species at these voltages suppresses O_2 formation by diverting $O(^3P)$ away from recombination pathways. At even higher voltages (approximately 23 V), filamentary discharges dominate the plasma. Under these conditions, the increased concentration of CO originating from CO_2 dissociation and partial oxidation of organics enhances three-body recombination reactions between CO, $O(^3P)$, and third-body collision partners, reforming CO_2. This further reduces the pool of atomic oxygen available for O_2 production, reinforcing the downward trend in the oxygen profile. The combined influence of radical consumption, localized heating, and intensified back-reactions explains the observed decline in O_2 concentration beyond the voltage optimum. The reaction process that occurs under these conditions can be summarized as follows(Korzec et al. 2025; Snoeckx and Bogaerts 2017):

$O(^3P) + H_2O \rightarrow 2OH(^2\Pi)$ (5)

$O(^3P) + VOCs \rightarrow$ oxidized organics (6)

$CO + O(^3P) + M \rightarrow CO_2 + M$ (7)

Overall, the oxygen formation characteristics in Fig. 1 reflect a dynamic competition between the production and consumption of atomic oxygen under varying discharge regimes. The early-time rise confirms that plasma enables immediate, non-equilibrium oxygen generation, while the voltage-dependent behavior highlights the critical balance between radical production in the diffuse regime and radical depletion in the filamentary regime. The optimum observed near 21–22 V represents the final stage where diffuse microdischarges still dominate, allowing efficient CO_2 dissociation and O_2 formation before high-voltage filamentation begins to suppress these pathways

Figure 2 shows a progressive decline in CO_2 concentration with increasing voltage, yet the slope of this decline changes distinctly across the applied voltage range. These changes reflect the transition of dominant mechanisms in the discharge, from low-energy electron-driven reactions to ionization-assisted

and radical-driven pathways at higher voltages. At low voltages (19–20 V), CO_2 dissociation proceeds primarily through vibrational excitation, where low-energy electrons promote CO_2 to its vibrational levels prior to bond cleavage, this mechanism is represented by reaction (8). However, vibrational quenching by water vapor and trace impurities in the flue gas reduces the lifetime of $CO_2(v)$, so the dissociation rates associated with reactions (1) and (2) remain limited at this stage. Consequently, the net CO_2 decline is relatively modest (Alliati et al. n.d.-c; Ola et al. 2023; Ponduri et al. 2016c).

A marked increase in CO_2 removal occurs between 21 and 22 V, which corresponds to an optimal electron energy distribution function (EEDF). In this region, a substantial fraction of electrons reaches the dissociation threshold without excessive ionization losses, and the discharge still operates predominantly in a diffuse regime. Multiple electron-impact pathways contribute concurrently, including direct dissociation (reactions (1) and (2)) and ionization-assisted routes (reactions (9) and (10)). The increased contribution of reactions (9) and (10) near 22 V produces the steepest decline in CO_2 concentration, establishing this voltage as the most effective dissociation window (Alliati et al. n.d.-b; Hayakawa et al. 2023b).

$CO_2 + e^- \rightarrow CO_2^* + 2e^-$ (9)

$CO_2^* + e^- \rightarrow CO + O$ (10)

$CO + OH \rightarrow CO_2 + H$ (11)

$CO_2^* + O \rightarrow CO^* + O_2$ (12)

When the applied voltage exceeds 22 V, the rate of CO_2 depletion starting to be flat. Several competing processes emerge at these higher fields. First, energy misallocation becomes increasingly significant: high-energy electrons increasingly favor ionization rather than dissociation, lowering the number of CO_2-breaking events per unit input energy. Second, moisture-induced quenching further suppresses vibrational excitation pathways such as reaction (8), reducing the overall dissociation efficiency. Finally, back-conversion of CO to CO_2 intensifies as radical concentrations in the filamentary regime. In particular, hot spots formed by filament channels promote reactions (11) and (4). These reverse pathways stop the net removal of CO_2 and add then to the plateau region that can be seen. Reaction (12) provides an additional fragmentation route once CO_2^* is produced, generating CO* and O_2 while simultaneously enhancing the pool of reactive oxygen species. Together, these reactions explain the steep decline in CO_2 concentration near 22 V, corresponding to the observed peak in O_2 formation and rapid increase in CO (Aerts et al. 2015b; Ray et al. 2017).

As illustrated in Fig. 3, the concentration of CO increases consistently with the applied voltage, reflecting the strong coupling between discharge power and CO_2 dissociation chemistry. The overall trend in CO formation closely mirrors the decline in CO_2 concentration presented in **Fig. 2**, especially in the 19–22 V range, indicating that the dominant source of CO is the electron-impact fragmentation of CO_2. In this voltage window, the electron energy distribution function (EEDF) becomes increasingly populated with

electrons capable of cleaving the C = O bond, promoting the dissociation channel represented by reaction (13):

$CO_2 + e^- \rightarrow CO + O$ (13)

This primary route efficiently generates CO together with ground-state atomic oxygen (O), which subsequently participates in the broader oxidation network discussed in earlier sections. At the lower voltages of 19–20 V, CO formation remains relatively modest because only a limited fraction of electrons attains the threshold energy necessary for reaction (13) to proceed at significant rates. In this diffuse micro-discharge region, electron densities and local temperatures remain moderate, and competing relaxation pathways such as vibrational quenching by water vapor further restrict the effective dissociation of CO_2. As a result, the incremental rise in CO remains small. However, once the voltage reaches the 21–22 V interval, the degree of electron energization becomes optimal for dissociation (Alliati et al. n.d.-c; Ponduri et al. 2016c).

Micro-discharges remain predominantly uniform, allowing the EEDF to sustain a high probability of electron-impact CO_2 splitting. Consequently, CO concentration increases sharply in this range, consistent with the region of highest CO_2 conversion efficiency identified in **Fig. 2.** Beyond approximately 22 V, however, the growth rate of CO begins to diminish despite increasing discharge power. This shift is primarily attributed to the intensification of back-reaction mechanisms that consume CO and reform CO_2. Two key reactions dominate this reverse pathway (Alliati et al. n.d.-b; Elaissi and Alsaif 2023; Mei et al. 2015; Shaban et al. 2024):

$CO + OH \rightarrow CO_2 + H$ (14)

$CO + O \rightarrow CO_2$ (15)

As the voltage increases, both O and OH become more abundant due to enhanced dissociation of CO_2 and H_2O, as well as contributions from ionization and excitation channels activated at higher energies. The accumulation of these reactive oxygen species accelerates reactions (14) and (15), effectively recycling part of the CO back into CO_2. This reformation process becomes increasingly significant in the filamentary discharge regime, where localized electric fields and transient hot spots favor rapid radical–radical and radical–molecule interactions. In addition to the back-reaction pathways, partially oxidized volatile organic compounds (VOCs) in the palm-biomass flue gas provide a secondary source of CO at elevated voltages. The transition toward filamentary discharges enhances the fragmentation of complex organics, producing small carbonaceous intermediates that can subsequently oxidize to CO. These VOC-driven pathways operate independently of CO_2 dissociation and thus partially counterbalance the CO losses caused by reactions (14) and (15). However, VOC fragmentation does not scale linearly with voltage, and its relative contribution becomes constrained once the plasma becomes dominated by high-energy filaments that reduce chemical selectivity. The onset of filamentary discharge above 22 V further alters the balance between CO formation and consumption (Aerts et al. 2015a; Alliati et al. n.d.-a). Filamentary channels exhibit elevated electron densities and temperatures, causing a shift in the EEDF

toward excessively energetic electrons. This shift reduces the relative efficiency of CO_2 dissociation while simultaneously increasing the probability of recombination reactions and radical scavenging processes. Hot spots within filaments facilitate rapid O and OH consumption, thereby promoting CO reoxidation through reactions (14) and (15), and contributing to the overall stabilization of CO concentration at higher voltages. Collectively, these interacting mechanisms produce the characteristic trend observed in Fig. 3: CO concentration increases nearly linearly within the 19–22 V range, where dissociation dominates, but the rate of increase slows beyond 22 V as back-reactions, radical quenching, and filament-induced recombination become more competitive. The system ultimately approaches a quasi-steady state where CO production derived from CO_2 dissociation (reaction 13) and VOC oxidation is progressively offset by CO-consuming reactions, leading to the attenuated slope in CO growth observed at the highest voltages (Ponduri et al. 2016b; Ray and Subrahmanyam 2016).

All possible reaction pathways occurring in the plasma within the 19–23 V voltage window were summarized in the following Table 1.

Table 1
Dominant Plasma Reaction Pathways and Discharge Characteristics

Voltage Range	Dominant Reactions	Likelihood	Notes (including discharge regime)
19 V	$CO_2 + e^- \rightarrow CO + O$	Medium	Diffuse regime (early). CO_2 dissociation begins but electron density is still modest. Moderate CO and O formation; O_2 remains low.
	$CO + O \rightarrow CO_2$	Medium	Back-reaction remains significant due to limited O availability and relatively low gas temperature.
	$O + O + M \rightarrow O_2$	Low-Medium	Three-body recombination limited by low O concentration; explains low O_2 signal at this voltage.
20 V	CO_2(v) vibrational ladder → dissociation	Medium–High	Diffuse regime with stronger microdischarges. Vibrational excitation begins to contribute significantly to net CO_2 splitting.
	$O + H_2O \rightarrow 2OH$	Medium	Humidity starts competing for O, slightly suppressing O_2 formation and redirecting chemistry toward OH-driven channels.
21 V	$CO_2 + e^- \rightarrow CO + O$	High	Upper diffuse regime (near-optimal E/N). EEDF overlaps CO_2 dissociation threshold efficiently; strong O production drives O_2 peak.
	$O + O \rightarrow O_2$	Medium–High	Two-body recombination increases sharply, consistent with O_2 maximum in the data.
	$CO + O \rightarrow CO_2$	Medium	Still competitive, but not strong enough to suppress CO accumulation observed in the conversion plot.
22 V	$CO_2 + e^- \rightarrow CO_2^+ + 2e^- \rightarrow CO + O$	High	Diffuse → pre-filament transition. Ionization-assisted dissociation becomes dominant; this voltage corresponds to peak CO_2 conversion.
	$OH + CO \rightarrow CO_2 + H$	Medium–High	OH-based back-reaction increases due to humidity; begins limiting further CO growth and partially restoring CO_2.
	VOC/tar oxidation → CO + organics	Medium	Secondary CO production via VOC oxidation starts to appear, consistent with biomass/plasma interactions.
23 V	High-energy electron impact ionization (less selective for dissociation)	Medium–High	Filament onset. EEDF shifts to high-energy tail; electrons waste energy on ionization rather than dissociation → CO_2 conversion plateaus/declines.

Voltage Range	Dominant Reactions	Likelihood	Notes (including discharge regime)
	$O^{*} + H_2O \rightarrow 2OH^{*}$	High	Strong O^{*} quenching suppresses O_2 formation and shifts chemistry toward OH production.
	$CO + O^{*} \rightarrow CO_2$	High	Back-reaction becomes dominant; explains the decline in CO accumulation beyond the optimum voltage.
	Thermal VOC/tar fragmentation → CO	Medium	Early thermal effects from proto-filament heating begin enhancing CO from cracking, partly compensating losses from back-reactions.

4. Conclusions

The findings indicate that 21 V represent the optimal operating condition for the dissociation of CO_2 and CO in oil palm empty-fruit-bunch (EFB) flue gas, considering the integrated trends of O_2 generation, CO reduction, and CO_2 conversion through the applied voltage range. This is confirmed from the combined trends of O_2 production, CO reduction, and CO_2 depletion across the applied voltage range. At this voltage, the discharge stays very even, which makes it easy for energy to move into CO_2 vibrational modes while yet being quite stable against changes caused by aerosols and impurities. Consequently, the dielectric barrier discharge (DBD) plasma effectively accelerates O_2 generation, limit CO concentration, and accomplishes substantial CO_2 conversion. These outcomes confirm the strong potential of DBD plasma as an advanced gas-cleaning technology for biomass-based industrial systems, particularly in the palm-oil sector. The study also reveals an important design insight: optimizing plasma reactors for biomass applications must take into consideration the complicated and reactive character of real flue-gas mixtures, not only data from idealized pure-gas settings. This kind of view is important for making plasma systems that can be used in industrial settings that are scalable and work well.

Declarations

Author Contributions: Rahmad Oktafiansyah: Conceptualization idea for the article, Software, Data Analysis, Writing - original draft preparation; **Gusti Atika Urfa**: Data Analysis, Writing; **Andi Tessiwoja Tenri Ola**: Data Analysis, Software, Visualization; Suryajaya: review and editing, Critically Revised the Work; **Muhammad Fadhil Syahputra**: Methodology, Software; **Muhammad Aghil Surya Syahputra**: Data Analysis, Writing - original draft preparation, Data Analysis; **Muhammad Afief Balya**: Methodology, Data Analysis.

Acknowledgements. The author would like to thank everyone and institutions that helped with this research. This work was done without any explicit financing from public or non-profit organizations.

Credit authorship contribution statement.

Data availability All data and materials generated or analyzed during this study are included in this article.

Ethics approval Not relevant.

All authors have read, understood, and complied, as applicable, with the statement on “Ethical responsibilities of authors” as found in the instructions for authors

Consent to participate Not relevant.

Consent for publication Not relevant.

Conflict of interest The authors declare no competing interests.

Funding Kementerian Pendidikan Tinggi, Sains, dan Teknologi.

Availability of data and materials the datasets used and/or analyzed during the current study are available from the corresponding author on reasonable request.

References

1. Aerts, R., Somers, W., & Bogaerts, A. (2015a). Carbon Dioxide Splitting in a Dielectric Barrier Discharge Plasma: A Combined Experimental and Computational Study. *ChemSusChem*, *8*(4), 702–716. https://doi.org/10.1002/cssc.201402818
2. Aerts, R., Somers, W., & Bogaerts, A. (2015b). Carbon Dioxide Splitting in a Dielectric Barrier Discharge Plasma: A Combined Experimental and Computational Study. *ChemSusChem*, *8*(4), 702–716. https://doi.org/10.1002/cssc.201402818
3. Alliati, M., Mei, D., & Tu, X. (n.d.-a). *Plasma activation of CO 2 in a dielectric barrier discharge: a 1 chemical kinetic model from the microdischarge to the reactor 2 scales 3*.
4. Alliati, M., Mei, D., & Tu, X. (n.d.-b). *Plasma activation of CO 2 in a dielectric barrier discharge: a 1 chemical kinetic model from the microdischarge to the reactor 2 scales 3*.
5. Alliati, M., Mei, D., & Tu, X. (n.d.-c). *Plasma activation of CO 2 in a dielectric barrier discharge: a 1 chemical kinetic model from the microdischarge to the reactor 2 scales 3*.
6. Al-Muraisy, S. A. A., Chuayboon, S., Soares, L. A., Buijnsters, J. G., Ismail, S. bin, Abanades, S., et al. (2025a). Carbon capture through solar-driven CO2 gasification of oil palm empty fruit bunch to produce syngas and biochar. *Energy*, *323*. https://doi.org/10.1016/j.energy.2025.135805
7. Al-Muraisy, S. A. A., Chuayboon, S., Soares, L. A., Buijnsters, J. G., Ismail, S. bin, Abanades, S., et al. (2025b). Carbon capture through solar-driven CO2 gasification of oil palm empty fruit bunch to produce syngas and biochar. *Energy*, *323*. https://doi.org/10.1016/j.energy.2025.135805
8. Bogaerts, A., Berthelot, A., Heijkers, S., Kolev, S., Snoeckx, R., Sun, S., et al. (2017, May 15). CO2 conversion by plasma technology: Insights from modeling the plasma chemistry and plasma reactor

design. *Plasma Sources Science and Technology*. Institute of Physics Publishing. https://doi.org/10.1088/1361-6595/aa6ada

9. Bogaerts, Annemie, Snoeckx, R., Trenchev, G., & Wang, W. (2018). Modeling for a Better Understanding of Plasma-Based CO2 Conversion. In *Plasma Chemistry and Gas Conversion*. IntechOpen. https://doi.org/10.5772/intechopen.80436
10. Bui, M., Adjiman, C. S., Bardow, A., Anthony, E. J., Boston, A., Brown, S., et al. (2018, May 1). Carbon capture and storage (CCS): The way forward. *Energy and Environmental Science*. Royal Society of Chemistry. https://doi.org/10.1039/c7ee02342a
11. Chai, S. Y. W., Ngu, L. H., & How, B. S. (2022, June 1). Review of carbon capture absorbents for CO2 utilization. *Greenhouse Gases: Science and Technology*. John Wiley and Sons Inc. https://doi.org/10.1002/ghg.2151
12. Chang, T., Wang, Y., Zhao, Z., Wang, Y., Ma, C., Gao, R., et al. (2022). Nonthermal plasma: An emerging innovative technology for the efficient removal of cooking fumes. *Journal of Environmental Chemical Engineering*, *10*(3). https://doi.org/10.1016/j.jece.2022.107721
13. Chen, Y., Shi, W., Li, C., Lim, K. H., Wang, X., Wang, L., et al. (2025). CO2 reduction by dielectric barrier discharge plasma in collaboration with Cu2 − xSe/AlO(OH) catalyst. *Journal of Materials Chemistry A*, *13*(12), 8445–8455. https://doi.org/10.1039/d4ta07805e
14. Dolah, R., Karnik, R., & Hamdan, H. (2021, September 1). A comprehensive review on biofuels from oil palm empty bunch (Efb): Current status, potential, barriers and way forward. *Sustainability (Switzerland)*. MDPI. https://doi.org/10.3390/su131810210
15. Elaissi, S., & Alsaif, N. A. M. (2023). Modelling of Nonthermal Dielectric Barrier Discharge Plasma at Atmospheric Pressure and Role of Produced Reactive Species in Surface Polymer Microbial Purification. *Polymers*, *15*(5). https://doi.org/10.3390/polym15051235
16. Golubev, O. V., Sadovnikov, A. A., & Maximov, A. L. (2025). Plasma-Activated CO2 Dissociation to CO in Presence of CeO2 Mesoporous Catalysts. *Molecules*, *30*(21). https://doi.org/10.3390/molecules30214312
17. Hayakawa, Y., Emeraldi, P., Imai, T., & Kambara, S. (2023a). CO 2 conversion characteristics by micro-gap DBD plasma reactorjp (Yukio Hayakawa). *Int. J. Plasma Environ. Sci. Technol*, *17*, 1007–1019. https://doi.org/10.34343/ijpest.2023.17.e01007
18. Hayakawa, Y., Emeraldi, P., Imai, T., & Kambara, S. (2023b). CO 2 conversion characteristics by micro-gap DBD plasma reactorjp (Yukio Hayakawa). *Int. J. Plasma Environ. Sci. Technol*, *17*, 1007–1019. https://doi.org/10.34343/ijpest.2023.17.e01007
19. Hong, W. O. (2023). Review on Carbon Footprint of the Palm Oil Industry: Insights into Recent Developments. *International Journal of Sustainable Development and Planning*, *18*(2), 447–455. https://doi.org/10.18280/ijsdp.180213
20. Jamaludin, N. F., Ab Muis, Z., Hashim, H., Mohamed, O. Y., & Lek Keng, L. (2024). A holistic mitigation model for net zero emissions in the palm oil industry. *Heliyon*, *10*(6). https://doi.org/10.1016/j.heliyon.2024.e27265

21. Kafı, M., Sanaeepur, H., & Ebadi Amooghin, A. (2023). Grand Challenges in CO2 Capture and Conversion. *Journal of Resource Recovery*, *1*(2), 0–0. https://doi.org/10.52547/jrr.2302-1007
22. Korzec, D., Freund, F., Bäuml, C., Penzkofer, P., Beier, O., Pfuch, A., et al. (2025). Hybrid Dielectric Barrier Discharge Reactor: Production of Reactive Oxygen–Nitrogen Species in Humid Air. *Plasma*, *8*(3). https://doi.org/10.3390/plasma8030027
23. Lindon, M. A., & Scime, E. E. (2014). CO2 dissociation using the Versatile atmospheric dielectric barrier discharge experiment (VADER). *Frontiers in Physics*, *2*, 1–13. https://doi.org/10.3389/fphy.2014.00055
24. Majesty, K. I., Purnamasari, B. D., Mizuno, K., Sutardi, T., & Ekawati, K. N. (2024). Palm Oil Waste Management with Local Wisdom as an Approach to Achieve Sustainable Development in Independent Smallholder Palm Plantations. *Evergreen*, *11*(4), 3484–3496. https://doi.org/10.5109/7326984
25. Mei, D., Zhu, X., He, Y. L., Yan, J. D., & Tu, X. (2015). Plasma-assisted conversion of CO2 in a dielectric barrier discharge reactor: Understanding the effect of packing materials. *Plasma Sources Science and Technology*, *24*(1). https://doi.org/10.1088/0963-0252/24/1/015011
26. Mei, D., Zhu, X., He, Y., Yan, J. D., Tu, X., & Uk, A. (n.d.). *Plasma-assisted conversion of CO 2 in a dielectric barrier discharge reactor: understanding the effect of packing materials CORE View metadata, citation and similar papers at core*.
27. Michielsen, I., Uytdenhouwen, Y., Pype, J., Michielsen, B., Mertens, J., Reniers, F., et al. (2017). CO2 dissociation in a packed bed DBD reactor: First steps towards a better understanding of plasma catalysis. *Chemical Engineering Journal*, *326*, 477–488. https://doi.org/10.1016/j.cej.2017.05.177
28. Moliner, C., Focacci, S., Antonucci, B., Moreno, A., Biti, S., Hamzah, F., et al. (2022). Production, Activation and CO2 Uptake Capacity of a Carbonaceous Microporous Material from Palm Oil Residues. *Energies*, *15*(23). https://doi.org/10.3390/en15239160
29. Mukhtar, A., Saqib, S., Mohotti, D., Ndeddy Aka, R. J., Hossain, M., Agyekum-Oduro, E., & Wu, S. (2024). Non-thermal plasma-catalytic processes for CO2 conversion toward circular economy: fundamentals, current status, and future challenges. *Environmental Science and Pollution Research*. Springer. https://doi.org/10.1007/s11356-024-34751-3
30. Nabila, R., Hidayat, W., Haryanto, A., Hasanudin, U., Iryani, D. A., Lee, S., et al. (2023, April 1). Oil palm biomass in Indonesia: Thermochemical upgrading and its utilization. *Renewable and Sustainable Energy Reviews*. Elsevier Ltd. https://doi.org/10.1016/j.rser.2023.113193
31. Oktafiansyah, R., Hanif, M. A., & D H Santjojo, D. J. (2022). *IMPROVING THE SWELLING EFFECT OF COPPER PHTHALOCYANINE SURFACES BY CONTROLLING SURFACE WETTABILITY AND MICROSTRUCTURE USING OXYGEN PLASMA TREATMENT*. *Romanian Journal of Physics* (Vol. 67).
32. Ola, A. T. T., Heryanto, H., Armynah, B., & Tahir, D. (2023, April 1). Bibliometric analysis of chitosan research for wastewater treatment: a review. *Environmental Monitoring and Assessment*. Springer Science and Business Media Deutschland GmbH. https://doi.org/10.1007/s10661-023-11094-z

33. Ozkan, A., Dufour, T., Bogaerts, A., & Reniers, F. (2016). How do the barrier thickness and dielectric material influence the filamentary mode and CO2 conversion in a flowing DBD? *Plasma Sources Science and Technology*, *25*(4). https://doi.org/10.1088/0963-0252/25/4/045016
34. Ponduri, S., Becker, M. M., Welzel, S., Van De Sanden, M. C. M., Loffhagen, D., & Engeln, R. (2016a). Fluid modelling of CO2 dissociation in a dielectric barrier discharge. *Journal of Applied Physics*, *119*(9). https://doi.org/10.1063/1.4941530
35. Ponduri, S., Becker, M. M., Welzel, S., Van De Sanden, M. C. M., Loffhagen, D., & Engeln, R. (2016b). Fluid modelling of CO2 dissociation in a dielectric barrier discharge. *Journal of Applied Physics*, *119*(9). https://doi.org/10.1063/1.4941530
36. Ponduri, S., Becker, M. M., Welzel, S., Van De Sanden, M. C. M., Loffhagen, D., & Engeln, R. (2016c). Fluid modelling of CO2 dissociation in a dielectric barrier discharge. *Journal of Applied Physics*, *119*(9). https://doi.org/10.1063/1.4941530
37. Purawiardi, I., Dimyati, A., Sari, Y. W., Elbersen, W., & Maddu, A. (2025). Conversion of some oil palm biomasses via plasma-assisted pyrolysis. In *Journal of Physics: Conference Series* (Vol. 2973). Institute of Physics. https://doi.org/10.1088/1742-6596/2973/1/012017
38. Ray, D., Saha, R., & Subrahmanyam, C. (2017). DBD plasma assisted CO2 decomposition: Influence of diluent gases. *Catalysts*, *7*(9). https://doi.org/10.3390/catal7090244
39. Ray, D., & Subrahmanyam, C. (2016). CO2 decomposition in a packed DBD plasma reactor: Influence of packing materials. *RSC Advances*, *6*(45), 39492–39499. https://doi.org/10.1039/c5ra27085e
40. Ren, L., Cheng, S., Xie, T., Zhang, Q., Li, R., Yue, T., & Cai, C. (2025, November 1). Low-Energy Regeneration Technologies for Industrial CO2 Capture: Advances, Challenges, and Engineering Applications. *Sustainability (Switzerland)*. Multidisciplinary Digital Publishing Institute (MDPI). https://doi.org/10.3390/su17219796
41. Sato, I., Listyanto, T., Susanti, A., & Kayo, C. (2025). Greenhouse gas emissions reduction potential of biomass power generation in Japan using empty fruit bunch pellets from Indonesia. *Tropics*, *34*(1), 11–22. https://doi.org/10.3759/tropics.MS24-04
42. Shaban, M., Merkert, N., van Duin, A. C. T., van Duin, D., & Weber, A. P. (2024). Advancing DBD Plasma Chemistry: Insights into Reactive Nitrogen Species such as NO2, N2O5, and N2O Optimization and Species Reactivity through Experiments and MD Simulations. *Environmental Science and Technology*, *58*(36), 16087–16099. https://doi.org/10.1021/acs.est.4c04894
43. Snoeckx, R., & Bogaerts, A. (2017, October 7). Plasma technology-a novel solution for CO2 conversion? *Chemical Society Reviews*. Royal Society of Chemistry. https://doi.org/10.1039/c6cs00066e
44. Soldatov, S., Link, G., Silberer, L., Schmedt, C. M., Carbone, E., D'Isa, F., et al. (2021). Time-Resolved Optical Emission Spectroscopy Reveals Nonequilibrium Conditions for CO2Splitting in Atmospheric Plasma Sustained with Ultrafast Microwave Pulsation. *ACS Energy Letters*, *6*(1), 124–130. https://doi.org/10.1021/acsenergylett.0c01983

45. Urfa, G. A., Amar, V., & Nasrulloh, N. S. (n.d.). *Jurnal Fisika Flux: Jurnal Ilmiah Fisika FMIPA Universitas Lambung Mangkurat Identifikasi Partikel Neutron Akibat Tembakan Proton pada Molekul Air*. https://physics.nist.gov/PhysRefData/Star/Text/PSTAR.html
46. Wang, W., Snoeckx, R., Zhang, X., Cha, M. S., & Bogaerts, A. (2018). Modeling Plasma-based CO2 and CH4 Conversion in Mixtures with N2, O2, and H2O: The Bigger Plasma Chemistry Picture. *Journal of Physical Chemistry C*, *122*(16), 8704–8723. https://doi.org/10.1021/acs.jpcc.7b10619
47. Wang, X., & Song, C. (2020a, December 15). Carbon Capture From Flue Gas and the Atmosphere: A Perspective. *Frontiers in Energy Research*. Frontiers Media S.A. https://doi.org/10.3389/fenrg.2020.560849
48. Wang, X., & Song, C. (2020b, December 15). Carbon Capture From Flue Gas and the Atmosphere: A Perspective. *Frontiers in Energy Research*. Frontiers Media S.A. https://doi.org/10.3389/fenrg.2020.560849
49. Zentou, H., Hoque, B., Abdalla, M. A., Saber, A. F., Abdelaziz, O. Y., Aliyu, M., et al. (2025, June 1). Recent advances and challenges in solid sorbents for CO2 capture. *Carbon Capture Science and Technology*. Elsevier Ltd. https://doi.org/10.1016/j.ccst.2025.100386

Figures

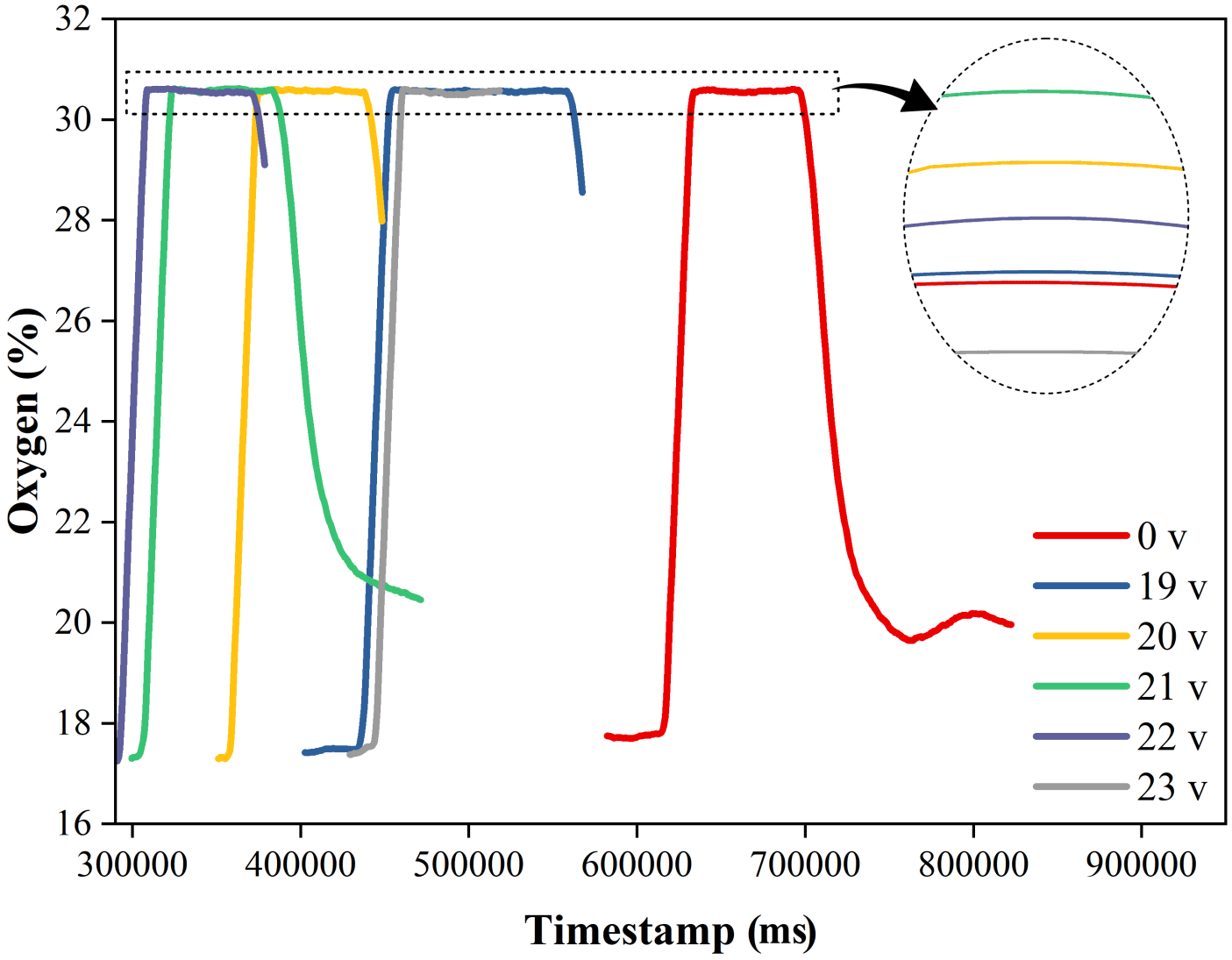


Figure 1

Behavior of Oxygen Formation Under Increasing Voltage

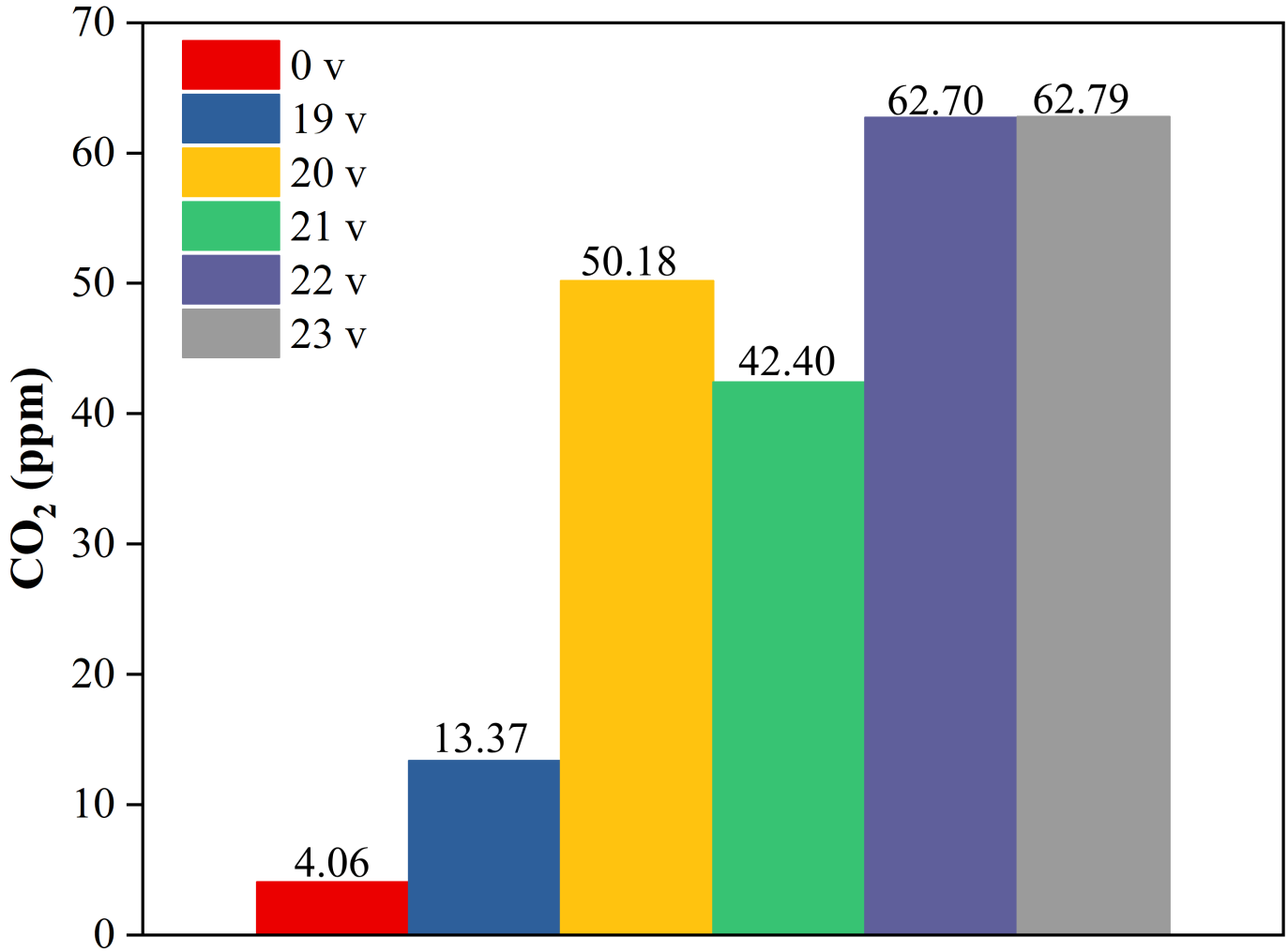


Figure 2

CO_2 Concentration and Its Voltage Dependence

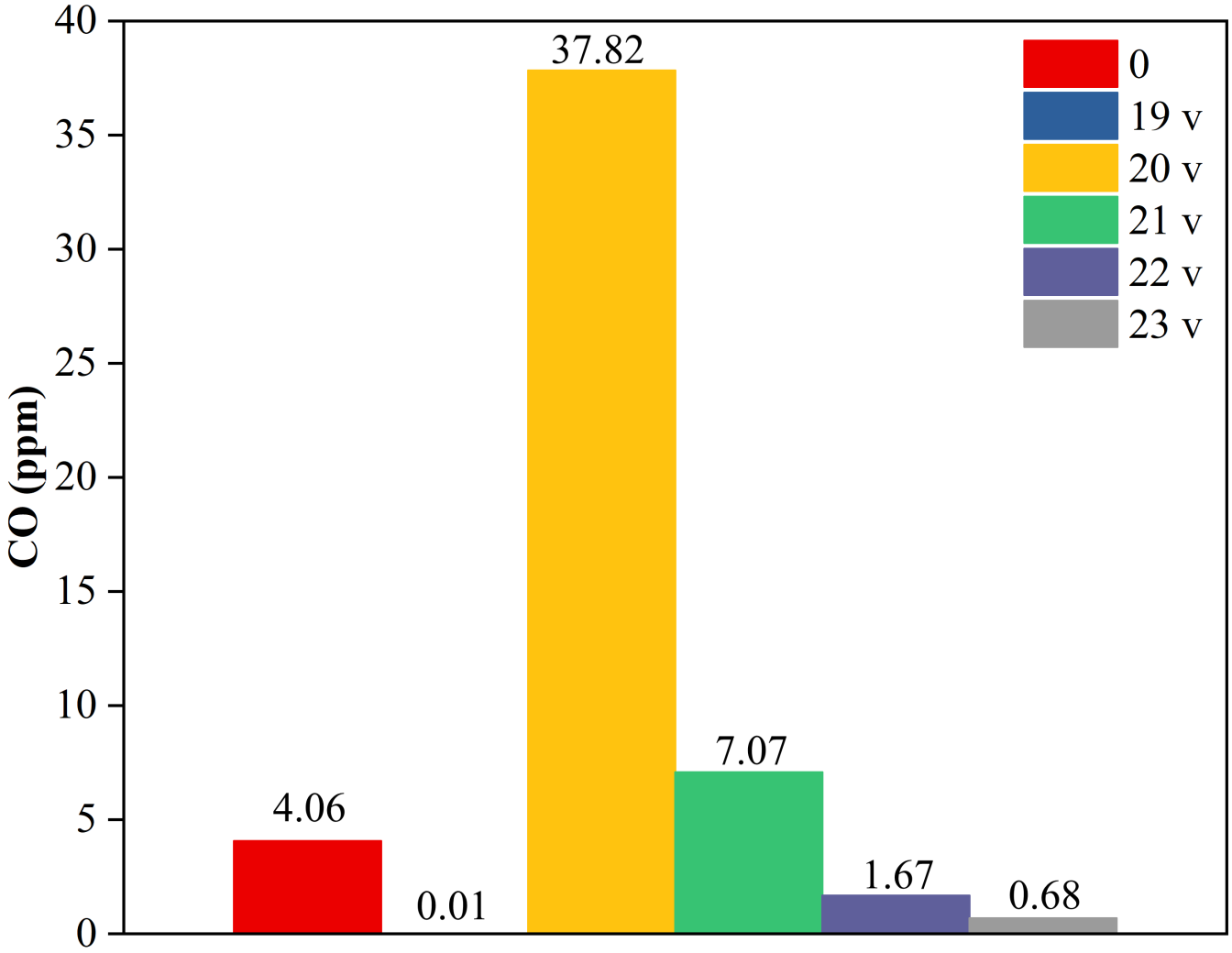


Figure 3

CO Formation and Trends Under Voltage Variation